



**HAL**  
open science

## Phosphorus retention by granulated apatite: assessing maximum retention capacity, kinetics and retention processes

Laura Delgado-González, Bruno Lartiges, Mathieu Gautier, Stéphane Troesch, Pascal Molle

### ► To cite this version:

Laura Delgado-González, Bruno Lartiges, Mathieu Gautier, Stéphane Troesch, Pascal Molle. Phosphorus retention by granulated apatite: assessing maximum retention capacity, kinetics and retention processes. *Water Science and Technology*, 2021, 83 (4), pp.792-802. 10.2166/wst.2021.010 . hal-04042976

**HAL Id: hal-04042976**

**<https://hal.inrae.fr/hal-04042976>**

Submitted on 23 Mar 2023





**HAL** is a multi-disciplinary open access archive for the deposit and dissemination of scientific research documents, whether they are published or not. The documents may come from teaching and research institutions in France or abroad, or from public or private research centers.

L'archive ouverte pluridisciplinaire **HAL**, est destinée au dépôt et à la diffusion de documents scientifiques de niveau recherche, publiés ou non, émanant des établissements d'enseignement et de recherche français ou étrangers, des laboratoires publics ou privés.



Distributed under a Creative Commons Attribution 4.0 International License

# Phosphorus retention by granulated apatite: assessing maximum retention capacity, kinetics and retention processes

Laura Delgado-González , Bruno Lartiges, Mathieu Gautier , Stéphane Troesch  and Pascal Molle 

## ABSTRACT

Natural apatites have previously shown a great capacity for phosphate retention from wastewater. However, its fine particle size distribution may lead to a premature clogging of the filter. Accordingly, a granulated apatite product was developed and manufactured in order to control the particle size distribution of the media. Experiments were conducted on laboratory columns to assess their phosphorus retention capacity, to identify the processes involved in phosphorus retention and to evaluate their kinetic rates. The results showed phosphorus retention capacities of 10.5 and 12.4 g PO<sub>4</sub>-P·kg<sup>-1</sup> and kinetic rate coefficients in the range of 0.63 and 0.23 h<sup>-1</sup> involving lower values than those found for natural apatites in previous studies. Scanning Electron Microscopy images showed that apatite particles in the granules were embedded in the binder and were not readily accessible to act as seeds for calcium phosphate precipitation. The retention processes differ depending on the supersaturation of the solution with respect to calcium phosphate phases: at low calcium concentrations (69.8 ± 3.9 mg·L<sup>-1</sup>), hydroxyapatite precipitates fill up the porosity of the binder up to a depth of 100–300 μm from the granule surface; at higher calcium concentrations (112.7 ± 7.4 mg·L<sup>-1</sup>) precipitation occurs at the granule surface, forming successive layers of hydroxyapatite and carbonated calcium phosphates.


**Key words** | granulated apatite filter, phosphorus retention, small WWTPs


## HIGHLIGHTS

- The kinetics and phosphorus retention capacity of granulated apatite are low and do not ensure long-term removal.
- Access to apatite surface in the granule is hindered by the binder matrix.
- Hydroxyapatite and carbonated-hydroxyapatite precipitate within the granule onto the binder matrix at low calcium concentration.
- Hydroxyapatite and carbonated-hydroxyapatite precipitate onto the granule surface at high calcium concentration.


This is an Open Access article distributed under the terms of the Creative Commons Attribution Licence (CC BY-NC-ND 4.0), which permits copying and redistribution for non-commercial purposes with no derivatives, provided the original work is properly cited (<http://creativecommons.org/licenses/by-nc-nd/4.0/>).

doi: 10.2166/wst.2021.010

Laura Delgado-González  (corresponding author)

Pascal Molle   
Inrae, REVERSAAL Research Unit,  
5 rue de la Doua,  
Villeurbanne 69100,  
France  
E-mail: [laura.delgado-gonzalez@inrae.fr](mailto:laura.delgado-gonzalez@inrae.fr)

Laura Delgado-González

Stéphane Troesch   
SYNTEA, Lieu-dit Belle-Croix,  
Le Pian sur Garonne 33490,  
France

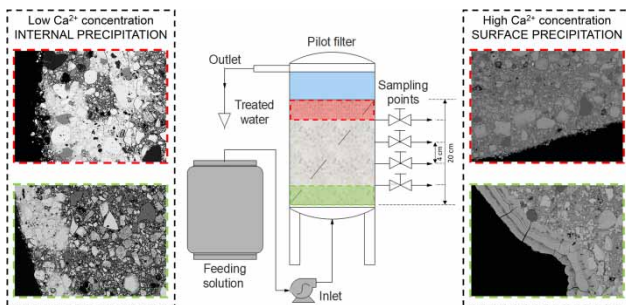
Bruno Lartiges

Géosciences Environnement Toulouse,  
University of Toulouse III (Paul Sabatier),  
14 av. Edouard Belin,  
Toulouse F-31400,  
France

Mathieu Gautier 

Univ Lyon, INSA Lyon, DEEP Laboratory,  
Villeurbanne 69100,  
France

## GRAPHICAL ABSTRACT



## INTRODUCTION

Phosphorus (P) is a key nutrient involved in eutrophication of surface waters (Prochaska & Zouboulis 2006). The major cause leading to the deterioration of water quality originates from anthropogenic sources such as municipal wastewater and runoff from agricultural areas (Bouwman *et al.* 2005). In all possible future scenarios, this pressure will continue to increase globally, demanding at least the implementation of additional treatments for phosphorus removal in wastewater treatment plants (WWTPs) (van Puijenbroek *et al.* 2019).

In small WWTPs, the addition of iron or aluminum salts to treat phosphorus is commonly used. Nevertheless, P removal remains a critical issue demanding the implementation of a supplementary treatment with simpler and more suitable technologies that can potentially meet P recovery purposes. Filtration through specific materials with an affinity for P binding appears to be an appropriate solution to reach these objectives. It also allows to maintain the extensive feature of treatment wetlands (TWs) (Molle *et al.* 2005) which represent more than 4,000 small WWTPs in France (Martinez-Carvajal *et al.* 2019). A large variety of filter substrates, from natural materials through man-made products to industrial coproducts, have been tested in laboratory, pilot and/or full-scale experiments in order to assess their P removal performance and retention capacities (Vohla *et al.* 2011; Yang *et al.* 2018). The adequacy of a given material for P retention is assessed from its phosphorus retention capacity (PRC), which depends on various physicochemical characteristics of the material (Blanco *et al.* 2016).

Previous studies have already demonstrated the validity of natural apatite as a specific filtering material for P retention (Molle *et al.* 2005; Bellier *et al.* 2006; Harouiya *et al.*

2011). Two different groups of natural apatite have been identified according to their fluorapatite content (FAP, Ca<sub>5</sub>(PO<sub>4</sub>)<sub>3</sub>F): poor quality (40–60% apatite content) and rich quality (90% apatite content). The latter substrate showed a great compromise in terms of performance, long term removal and potential capacity for P recovery (Molle *et al.* 2011). The main drawback of such material is its fine particle size distribution (Molle *et al.* 2011), which may cause hydraulic limitations for its applicability in wastewater treatments. Accordingly, a granulated apatite product was developed, patented and manufactured in a similar way as fertilizer pellets, by using a cement binder (10% w/w) and a natural source of apatite from phosphate rocks. The granulation allows control of the particle size distribution of the filtration bed and, thus, ensures a safer filtration operation regarding the filter hydraulics.

P retention using specific materials is a physicochemical process based on various interactions at the solid-liquid interface. For natural apatite, the surface reactions previously identified were adsorption and precipitation (Molle *et al.* 2005). The adsorption takes place at the beginning of the filter's lifespan onto Ca oxides' specific sites of phosphate minerals (Molle *et al.* 2005). As those sites become saturated, precipitation takes over as the long-term mechanism governing the P retention process (Molle *et al.* 2011). Mineral apatite was shown to act as a crystallization seed promoting calcium phosphate (CaP) precipitation such as hydroxyapatite (HAP, Ca<sub>5</sub>(PO<sub>4</sub>)<sub>3</sub>OH) (Molle *et al.* 2005; Bellier *et al.* 2006).

Precipitation is a thermodynamically driven process that depends on the solubility of the most stable pure solid phase and the free energy change. In a CaP system, the most stable solid phase is hydroxyapatite (HAP, Ca<sub>5</sub>(PO<sub>4</sub>)<sub>3</sub>OH) followed

by octocalcium phosphate (OCP), tricalcium phosphate (TCP) and dicalcium phosphate (DCP), among the most common CaP, depending on their solubility product ( $K_{sp}$ ) (Song *et al.* 2002a, 2002b). The saturation index (SI) of a solution determines whether a specific CaP phase may precipitate ( $SI > 0$ ).

However, kinetic and mechanistic factors also play a major role in the nucleation and the growth of solid solutions and may determine their crystal composition (Prieto *et al.* 2016). The kinetics of precipitation is supersaturation dependent: the induction time for crystallization decreases with increasing supersaturation (Anderson & Rubin 1981). In addition, for a particular supersaturation state, precipitation may or may not take place depending on environmental conditions because of the existence of a metastable zone (Song *et al.* 2002a, 2002b). Therefore, the rate of crystallization and nature of the phases that may precipitate strongly depend on calcium and phosphate concentrations, supersaturation, ionic strength, temperature, pH, the presence of foreign ions and time to enable solid-to-solid transformations (Barone & Nancollas 1977; Montastruc *et al.* 2003).

In this work, a transformed apatite-based product is analyzed in laboratory columns for P retention for the first time. The study intends to assess the suitability of the granulated apatite for phosphorus removal from wastewaters of small WWTPs, which would provide the advantages of extensive systems, requiring simple management and offering a final product that can be revalorized in the fertilizer industry. Therefore, the objectives of this work are: (1) to assess the PRC of a granulated apatite product using long-term column experiments; (2) to evaluate the kinetic rate of the reactions and its evolution with PRC using a simplified reaction rate model; (3) to identify the reaction processes taking place under various solution conditions and their impact in the PRC and the reaction rate; (4) to assess the adequacy of the granulated apatite filter for a long-term P retention.

## MATERIALS AND METHODS

### Characteristics of granulated apatite

The granulated apatite product was specifically designed to be used as a filtering material for P retention in wastewater. It was developed, patented (Blandin 2013) and manufactured by a French fertilizer company, which provided the product for this study.

A physicochemical and mineralogical characterization of the raw granulated apatite was carried out. Elemental analyses were carried out by alkaline fusion ( $LiBO_2$ ) followed by acid

digestion ( $HNO_3$ ) and subsequent analyses of the solutions by inductively coupled plasma optical emission spectrometry (ICP-OES) (iCap6500, Thermo Scientific). The mineralogical characterization was carried out on raw dried ground ( $80 < \mu m$ ) samples by X-ray diffraction (XRD) with a  $CuK\alpha$  radiation ( $\lambda = 1.54060 \text{ \AA}$ ) on a  $2\theta$  diffractometer (Bruker D8-Advance) in the  $5\text{--}70^\circ$  range. Crystalline phases were identified using DIFFRAC EVA software (v.4.1.1) by comparing the registered patterns with the Powder Diffraction Files (PDF).

The crystallographic microstructure and the chemical composition of the raw granulated material and of the precipitates after experiment were also investigated. The apatite granules were first embedded in an epoxy resin to obtain cylindrical resin blocks (4 cm in diameter), which were abraded and polished in ethanol using successively finer silicon carbide powders. Finally, an ethanol-based diamond slurry was used to produce a smooth polished finish suitable for recording Electron Backscatter diffraction patterns. The polished sections were carbon coated and examined by Scanning Electron Microscopy (SEM JEOL JSM-7100) equipped with an Electron Backscattered Diffraction pattern detector (EBSD AZtec HKL) and an Energy Dispersive X-ray analyser (EDS Oxford Instruments) for microanalysis (R. Castaing Microcharacterization Centre, France).

SEM-EDS images of the granule surface before and after the experiment were also carried out with a SEM-EFG XL30 Philips microscope. In that case, samples were gold coated to avoid surface polarization.

The Specific Surface Area (SSA) was determined by  $N_2$  adsorption/desorption isotherms (BET method) using an ASAP 2020M.

### Column experiments setup

The granulated apatite material was tested in two columns of 9 cm diameter and 20 cm of filter media depth (void volume of 0.62 L). The columns have equidistant depth sampling points, which enable solution sampling at various retention times. The system operated hydraulically saturated in a vertical and controlled up-flow regime (peristaltic pump). The columns were covered with a black opaque plastic coating in order to avoid algae development in the media. A schematic representation of the laboratory columns used for the experiments is presented in Figure 1.

### Feeding and analyses protocol

Several-month experiments were carried out in two columns: Column 1 and Column 2 (Table 1). Both filters

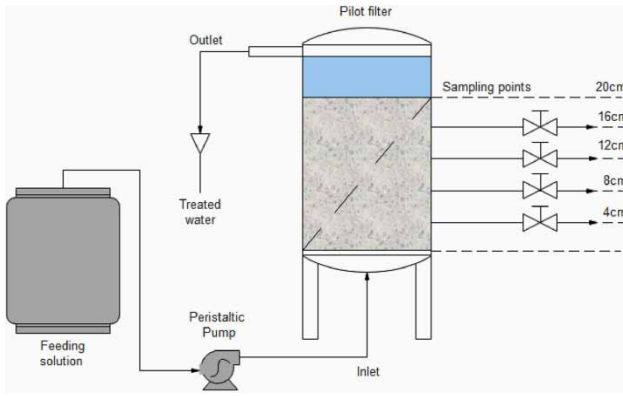


**Figure 1** | Schematic representation of laboratory columns.

**Table 1** | Composition of the feeding solutions and operational conditions for both Columns 1 and 2.

	Column 1 (low Ca <sup>2+</sup> concentration)	Column 2 (high Ca <sup>2+</sup> concentration)
[P-PO <sub>4</sub> <sup>3-</sup> ] (mg·L <sup>-1</sup> )	14.8 ± 1.2 (46)	12.6 ± 2.9 (33)
[HCO <sub>3</sub> <sup>-</sup> ] (mg·L <sup>-1</sup> )	197 ± 14 (63)	182 ± 14 (45)
[Ca <sup>2+</sup> ] Stage 1 (mg·L <sup>-1</sup> )	69.8 ± 3.9 (63)	112.7 ± 7.4 (34)
[Ca <sup>2+</sup> ] Stage 2 (mg·L <sup>-1</sup> )	69.8 ± 3.9 (63)	67.3 ± 3.9 (11)
Conductivity (μS·cm <sup>-1</sup> )	1,047 ± 63 (65)	1,047 ± 76 (45)
pH	7.5 ± 0.2 (65)	7.7 ± 0.2 (45)
Flow-rate Stage 1 (L·day <sup>-1</sup> )	5.1 ± 0.3 (391)	9.6 ± 2 (304)
Flow-rate Stage 2 (L·day <sup>-1</sup> )	10.2 ± 0.6 (76)	9.6 ± 2 (304)
Hydraulic load Stage 1 (m <sup>3</sup> ·m <sup>-2</sup> ·day <sup>-1</sup> )	0.80 ± 0.05 (391)	1.51 ± 0.31(304)
Hydraulic load Stage 2 (m <sup>3</sup> ·m <sup>-2</sup> ·day <sup>-1</sup> )	1.6 ± 0.09 (76)	1.51 ± 0.31(304)
Hydraulic retention time Stage 1 (h)	2.9 ± 0.2 (391)	1.6 ± 0.7 (304)
Hydraulic retention time Stage 2 (h)	1.5 ± 0.1(76)	1.6 ± 0.7 (304)
Experimental time_Stage 1 (days)	391	242
Experimental time_Stage 2 (days)	77	72
P-dosed_Stage 1 (kg·m <sup>-3</sup> material)	35.1	35.8
P-dosed_Stage 2 (kg·m <sup>-3</sup> material)	50.2	48.2

Mean value ± Standard deviation (95%) and number of samples analysed in brackets.

were fed with a synthetic solution prepared from tap water and KH<sub>2</sub>PO<sub>4</sub> (Sigma-Aldrich) to achieve phosphorus inlet concentrations around 15 mg P-PO<sub>4</sub>·L<sup>-1</sup>. The conductivity was also adjusted by adding a NaCl solution (common

salt, 300 mg·L<sup>-1</sup>) to approach common values in real wastewater (≈1,000 μS·cm<sup>-1</sup>). To investigate the influence of various parameters, the experiments were conducted in two different stages. For Column 1, flow rate was set approximately at 5 L·d<sup>-1</sup> during Stage 1 and 10 L·d<sup>-1</sup> during Stage 2 in order to reach the maximum PRC within the experimental time. The corresponding hydraulic loads used, also presented in Table 1, are in the range of hydraulic loads for full-scale systems. For Column 2, the flow rate was kept constant at approximately 10 L·d<sup>-1</sup> through the whole experiment. However, the calcium concentration was adjusted to 113 ± 7 mg·L<sup>-1</sup> by the addition of CaCl<sub>2</sub> (Sigma-Aldrich) during stage 1 of Column 2. This allowed study of the influence of calcium concentration in the reaction processes and kinetics. During Stage 2 of Column 2, the calcium concentration was kept equal to 70 ± 4 mg·L<sup>-1</sup>, as for both stages of Column 1. Therefore, in Stage 2, the experimental conditions of both columns were the same.

Samples were collected once a week at the inlet and outlet of the systems. To assess the evolution of P concentration inside the filtering media, samples were also collected at the different sampling points of the column, spaced 4 cm from each other, at selected times of the experiment. Calcium and phosphate concentrations were analyzed on filtered samples (pore size 0.45 μm) by ionic chromatography (NF EN ISO 14911 and EN ISO 10304-1). Both conductivity and pH were measured for each sample. The flow rate was checked every two days and adjusted when necessary.

The saturation indexes (SI) of the inlet solution for the minerals considered were calculated using the geochemical software PHREEQC v.3 (Parkhurst & Appelo 2013) using the LLNL database modified to take into account the K<sub>sp</sub> of the different minerals according to Song *et al.* (2002a, 2002b).

### The k-C\* model

The results were adjusted to the slightly modified k-C\* model (Equation (1)) (Kadlec & Wallace 2009).

$$C = (C_0 - C^*)\exp(-k_v t) + C^* \quad (1)$$

Where  $C$  is the  $P$  concentration at time  $t$ , or hydraulic retention time (HRT),  $C_0$  is the inlet concentration of phosphorus,  $k_v$  the volumetric kinetic rate coefficient and  $C^*$  the  $P$  equilibrium concentration.

Several kinetic studies were performed through the experiment at different PRC in both Columns 1 and 2. The

evolution of P concentration was then analyzed within the column by sampling at different hydraulic retention times (HRT) to determine the parameters of the  $k-C^*$  model (Kadlec & Wallace 2009). Consecutive kinetics studies were carried out by progressively reducing the inlet P concentration to reproduce several piston reactors in series. This allows better definition of  $k_v$  at high inlet concentration and  $C^*$  when approaching low P inlet concentrations.

## RESULTS AND DISCUSSION

### Material characterization

The granulated apatite was found to contain about 12%wt of P and 79%wt of apatite content. Such content falls between poor and rich quality in the classification of natural apatites for filtering media proposed by Molle *et al.* (2011) (Table S1). The XRD analyses revealed that the apatite phase present in the granulated apatite is a carbonate fluorapatite (CFAP) (Table S1).

The raw granulated apatite also contained high amounts of Ca (32.6%wt) that may be present in the CFAP, in calcite (12.4%wt), and to a lesser extent in dolomite (3.1%wt) (Table S2). Some quartz particles were also present at low concentrations (4.8%wt). The amorphous phases were not identified; however, their composition is likely derived from the cement binder used for granulation, whose elemental composition was determined by ICP spectrometry (Table S2).

SEM images and EDXS microanalyses further confirm the presence of various mineral phases previously identified by XRD analyses, and provide a description of the granule morphology. Figure 2(a) reveals particles of 20 to 100  $\mu\text{m}$  in size embedded in a binder matrix with micrometric to

sub-micrometric particles and the presence of a highly porous network. The brightness of particles is related to their average atomic number, thus identifying a vast majority of apatite particles (light grey to white) with minor occurrences of calcite (grey), quartz (dark grey) and dolomite.

Enlarged micrographs of the composite matrix (Figure 2(b)) reveal that the binder matrix is formed of nanoparticles, 30–200 nm in diameter, partially covering the apatite particles. The inset in Figure 2(b) shows the porosity of the granules at the external surface. In the following, the interconnected pore space developed by the binder and the particles within the granules is called the internal porosity of the granules or granules porosity. It differentiates from the pore space developed by a bed of granules, or bed porosity.

The BET measurement indicates a relatively high specific surface area (SSA) of about  $32 \text{ m}^2 \cdot \text{g}^{-1}$  (see Table S3 for a detailed comparison with other filtering materials used for P retention). The sorption capacity is strongly correlated with SSA and particle size distribution: high SSA and fine particles normally lead to a high PRC. The particle size distribution of the granulated apatite product does not show the presence of fine particles. Hence, the large SSA likely results from both the highly porous network of the granulated apatite pellets and the nanoparticles of the binder matrix observed from SEM micrographs (Figure 2(b)).

### Column experiments

#### Maximal retention capacity

The amount of P retained per amount of phosphorus entering the filter for both columns 1 and 2 is shown in Figure 3. P retention performances seem to reach an asymptotic trend, with Column 2 showing a slight improvement on P retention performance compared to Column 1. Data

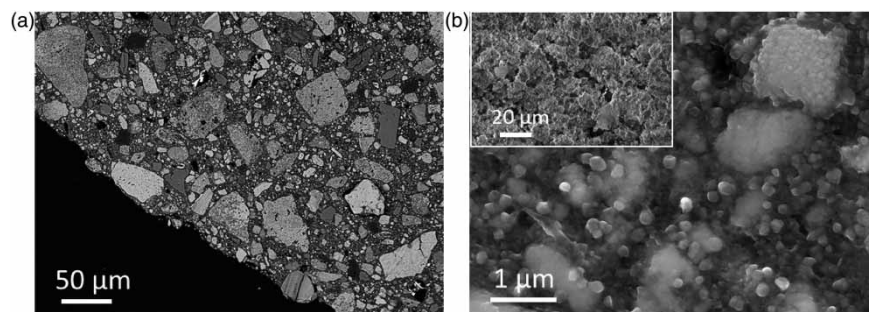


**Figure 2** | SEM micrographs of polished cross-section of a raw granulated apatite pellet (left): (a) Edge of a granule in backscatter electron mode revealing mostly apatite particles embedded in a composite matrix. (b) Micrograph of the matrix in the secondary electron mode showing that the binder is formed of nanoparticles; the inset shows the external surface of the pellet.

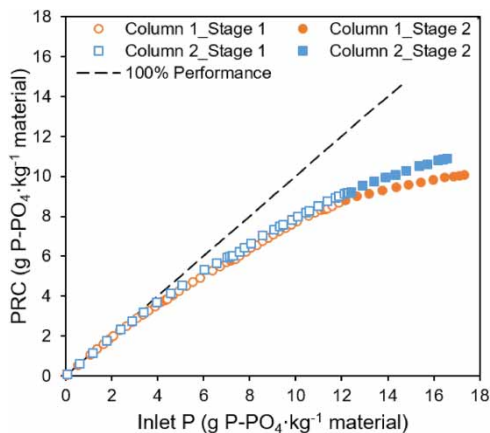


**Figure 3** | Evolution of phosphorus retention performance for columns 1 and 2. The plot compared their performance to the line of 100% and shows the correlation equations for the estimation of their maximum PRC.

showed performances decreasing under 90% from just 2.3 and 2.8 g P-PO<sub>4</sub>·kg<sup>-1</sup> material and estimated maximum PRCs at 10.5 g P-PO<sub>4</sub>·kg<sup>-1</sup> material and 12.4 g P-PO<sub>4</sub>·kg<sup>-1</sup> material for Columns 1 and 2, respectively (Table S4).

Molle *et al.* (2005) carried out long-term experiments with rich quality natural apatite, attaining a retention capacity of 13.9 g P-PO<sub>4</sub>·kg<sup>-1</sup>, where the material performance for P retention was still greater than 90% at the end of the experiment. Therefore, the maximal retention capacity of granulated apatite appears relatively low compared to that of natural apatite.

### Estimation of kinetic parameters

Similarly to natural apatite, the evolution of kinetic rate coefficient with P retention capacity in granulated apatite (Figure 4) reveals the presence of two different processes for phosphorus retention (Molle *et al.* 2005). High kinetic rate coefficients at the beginning of the filter's lifespan is attributed to the presence of adsorption reactions (Molle *et al.* 2005). As precipitation becomes the predominant mechanism, the kinetic rate coefficient decreases to attain a pseudo stabilization. For dimensioning purposes based on a long-term retention, the mean  $k_v$  value during the precipitation phase is therefore an important parameter. Thus, a substrate with a high stabilized kinetic coefficient (for high PRC) should be favored in order to have high P retention rates.

Previous studies have pointed out that the apatite content in the filtering material significantly affects the kinetic rate and hence the removal efficiency (Molle *et al.* 2011). The evolution of the kinetic rate coefficient with P retention capacity of the two columns was compared with natural

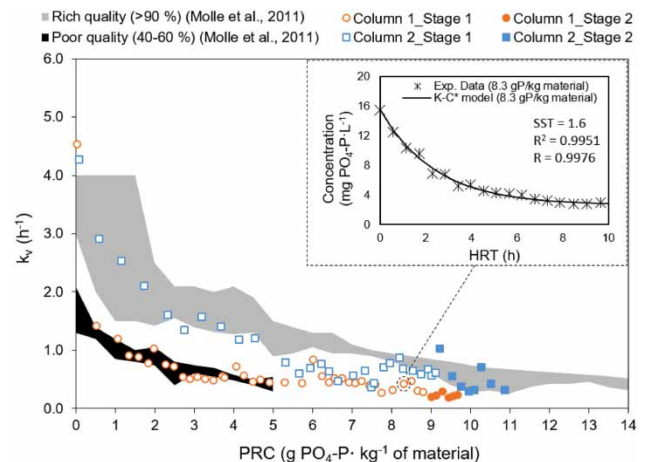


**Figure 4** | Evolution of kinetic coefficients with media PRC for both columns and comparison to natural apatite from Molle *et al.* (2011) (shaded area) showing lower  $k_v$  values than rich quality apatite. The insight shows an example of the adjustment of experimental data to  $k$ - $C^*$  model to determine  $k_v$  and  $C^*$ . The adjustment of the data was verified by the calculation of the sum of square errors (SSE), the coefficient of determination ( $R^2$ ) and the correlation coefficient ( $R$ ).

substrates of rich and poor apatite content. Figure 4 indicates that  $k_v$  of Column 1 evolves similarly to what is observed for a natural apatite material of poor quality. On the other hand, the calcium addition in Column 2 leads to higher  $k_v$  values characterizing a trend half way between poor and rich-quality natural apatites. The mean  $k_v$  value during precipitation is 0.63 h<sup>-1</sup> for Stage 1 and 0.41 h<sup>-1</sup> for Stage 2. For Column 1, the mean  $k_v$  values determined are 0.48 h<sup>-1</sup> and 0.23 h<sup>-1</sup> for Stages 1 and 2, respectively.

The impact of calcium addition in Column 2 during Stage 1 leads to an improved retention rate with regards to Column 1 in spite of the more demanding hydraulic conditions. This evidences that calcium concentration may be a limiting factor in CaP retention rates even when enough Ca concentration is provided ( $Ca/P > 1.67$  in both cases). A higher calcium concentration increases supersaturation, resulting in an increase in the crystal growth rate (Peng *et al.* 2018). During Stage 2, on the other hand, both columns share the same operational conditions but  $k_v$  for Column 2 is almost twice that of Column 1. This may indicate that different processes occurred during the preceding stage leading to significantly different kinetic rates. These aspects will be discussed more precisely from the examination of the SEM images.

### Estimation of background concentration

The evolution of  $C^*$  with PRC is also an important parameter to assess, since it determines the lowest P

concentration achievable for a given filtering material under given solution conditions. Figure 5(a) shows how  $C^*$  strongly increases with the retention capacity of the media, under the operational conditions of Column 1. Using the correlation, it can be estimated that outlet concentrations will exceed 1 and 2 mg P- $PO_4$ -L $^{-1}$  for PRCs around 4 and 10 g P- $PO_4$ -kg $^{-1}$  of material, respectively. Therefore, the substrate may not ensure low concentration discharge restrictions over a long-term retention. Instead, for Column 2 (Figure 5(b)),  $C^*$  evolves with a logarithmic trend that stabilizes close to 1 mg P- $PO_4$ -L $^{-1}$  once the adsorption phase is over. Therefore, P retention for such particular feeding conditions appears to have a weak dependence on the PRC of the media for the range considered. This might be explained by the increment in supersaturation due to calcium addition, which makes precipitation less dependent on the catalytic properties of the material but on the solution properties.

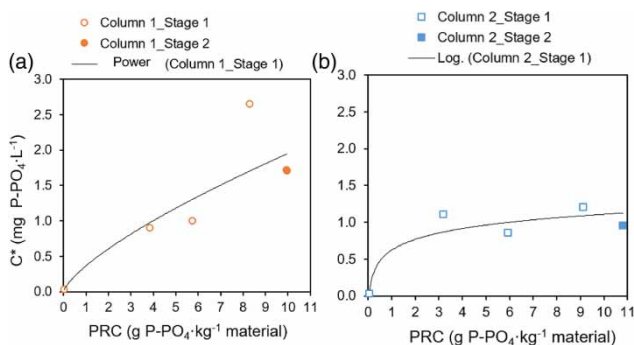


**Figure 5** | Evolution of  $C^*$  parameter with PRC for Column 1 (a) showing a power-like correlation and for Column 2 (b) showing a logarithmic evolution.

### Factors affecting CaP precipitation

The level of supersaturation in solution may have played a key role in the experimental results. Some aspects, like pH or Ca/P molar ratio, affect the supersaturation ratio and hence the kinetics of the process.

Precipitation of HAP should imply a pH decrease in solution (Blanco *et al.* 2016). However, no pH decrease could be observed during the whole experiment for the system in Column 1. In contrast, for Column 2, a pH decrease occurs several times during the experiment. Such discrepancy may be explained by the occurrence of distinct P retention processes for the two systems.

On the other hand, the initial Ca/P molar ratio in solution plays an important role in the crystallization, since it affects the efficiency of precipitation and the elemental composition of the crystal product (Peng *et al.* 2018). Mean inlet Ca/P ratio is  $3.7 \pm 0.4$  for Column 1 during Stages 1 and 2, and  $7.9 \pm 3.6$  and  $3.9 \pm 0.5$  for Column 2 during Stage 1 and Stage 2, respectively. This resulted in a lower Ca/P ratio retained (Equation (2)) on average for Column 1 than for Column 2 Stage 1 (Figure 6). The Ca/P ratio retained was compared with the CaP phases more likely to precipitate. For Column 1, the average Ca/P molar ratio retained in the column is lower than any of the possible stoichiometric CaP phases. On the contrary, higher Ca/P ratios were achieved for Column 2 during both Stages 1 and 2.

$$\left(\frac{Ca}{P}\right)_{\text{retained}} = \frac{[Ca^{2+}]_{\text{in}} - [Ca^{2+}]_{\text{out}}}{[P - PO_4^{3-}]_{\text{in}} - [P - PO_4^{3-}]_{\text{out}}} \quad (2)$$

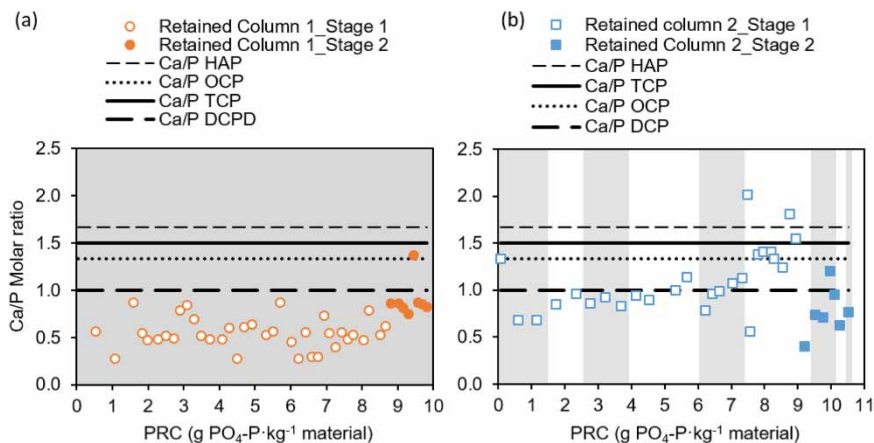


**Figure 6** | Evolution of the average Ca/P molar ratio of the column with media saturation for Column 1 (a) and Column 2 (b). The grey shaded areas indicate the regions where acidification did not occur during the process.



A mean retained Ca/P ratio may give an idea of how much impact inlet conditions have on P retention. However, as Ca and P are being consumed, supersaturation and Ca/P ratio in solution evolve in the bulk of the column (Figure S1). CaP precipitation through the column induces an increase in Ca/P ratio of the solution with the HRT. On the contrary, supersaturation is greater close to the system's inlet and therefore, most of the P precipitation will take place there. The mean Ca/P ratio retained will neither account for dissolution nor re-precipitation processes that may take place inside the column. Therefore, the speciation of CaP phases and its evolution (solid to solid transformations) may vary in time and space as a function of the media depth (Montastruc *et al.* 2003).

The saturation indexes for several calcium phosphates and calcite were determined for the three different inlet solution conditions (Table S5). Results indicated supersaturation with respect to HAP, OCP and TCP for all inlet solutions and undersaturation for DCP, while calcite shows SI values close to equilibrium ( $SI = 0$ ) (Table S6). Several authors have already reported that some species such as TCP or OCP may act as precursors or metastable phases for HAP precipitation (Montastruc *et al.* 2003; Blanco *et al.* 2016). Following the Ostwald step rule (Van Santen 1984), the sequence for Ca/P precipitation starts with the more soluble species, which then undergoes several dissolution/recrystallization processes until the most stable phase is formed (Montastruc *et al.* 2003; Han *et al.* 2016; Prieto *et al.* 2016). Thus, in the systems being considered, the theoretical sequence for Ca/P precipitation would be: TCP, OCP and HAP for both columns. Actually, slightly greater SI values were found for Column 2, which may explain the higher kinetic rates observed.

### Identification of retention processes

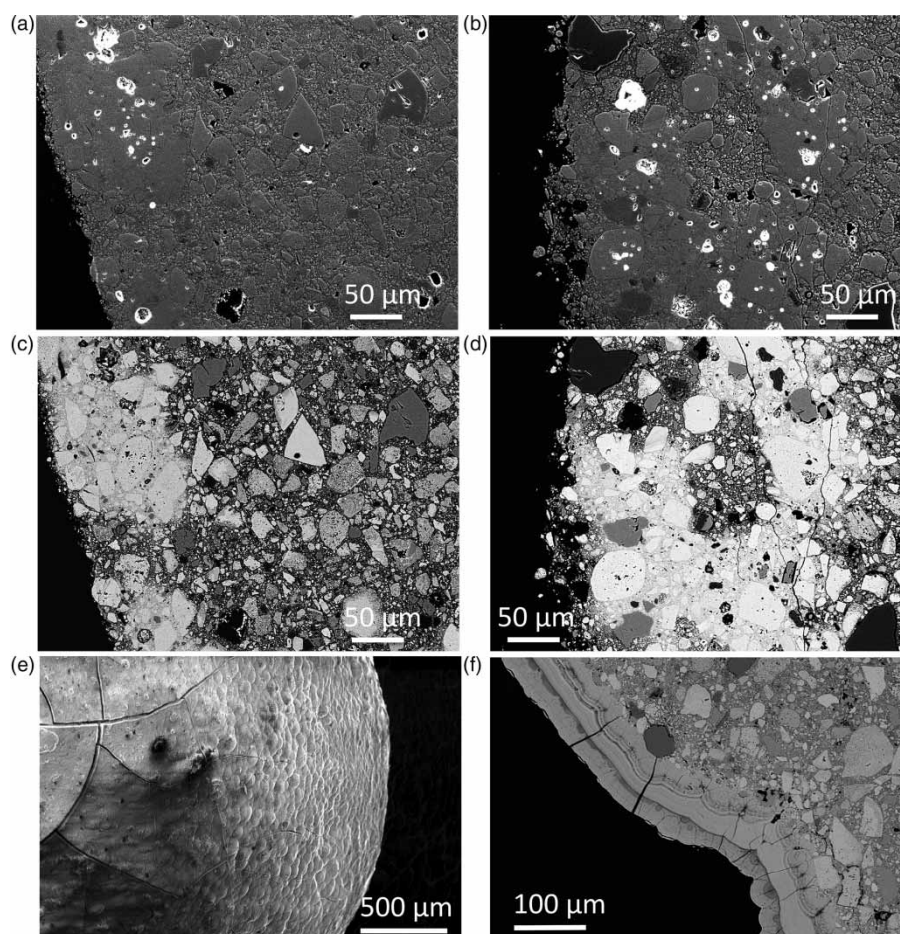
Results concerning the retention performance and the kinetic aspects have shown a media with low PRC and low kinetic rates. SEM observations coupled with EDS analyses allow unveiling of the P retention processes associated with these features and comparison with those determined for mineral apatite, as well as the influence of Ca addition on them.

Figure 7(a)–7(d) show SEM micrographs of polished cross-sections of granules collected at the end of the experiment either at the bottom (a, c) or at the top (b, d) of Column 1. Micrographs (Figure 7(a) and 7(b)) reveal that part of the porosity in the vicinity of the granule edge has been irregularly clogged to a depth of 100 to 300  $\mu\text{m}$  (Figure S2(b)). The clogged region viewed in the backscattered electron mode (Figure 7(c) and 7(d)), appear in a

light grey shade close to that of apatite particles, which suggests an equivalent chemical composition. EDXS microanalyses lead to a Ca/P elemental ratio of about 1.7, which confirms a precipitation of hydroxyapatite in the internal porosity of the granule. Close examination of clogged regions showed that the binder matrix is evenly coated with the precipitate, whereas unclogged regions look similar to the initial raw material with Ca/P ratio remaining in the 1.8–2.2 range (Figure S2(a)). Thus, it appears that adsorption and precipitation phenomena are not carried out at the interface of the large apatite particles present in the granule, but within the binder matrix itself. Indeed, the apatite particles are almost completely surrounded by other particles and the binder, which prevent ions to have an easy access to the apatite mineral surface. As a consequence, the precipitate essentially fills up the binder porosity.

Two hypotheses may account for the phosphorus retention under the operational conditions of Column 1. First, the presence of micrometric to sub-micrometric apatite particles in the binder matrix which may act as seeds for CaP precipitation. Then, local increases in supersaturation at the pore scale due to the dissolution of calcium containing minerals present in the binder, which would facilitate precipitation by increasing the reaction rates. In both cases, the diffusion rates within the pore are expected to be lower than adsorption and precipitation rates, which added to the tortuosity of the pores, results in a restricted penetration of phosphate ions in solution along the pores into the granule. A reduction of the binder porosity of the granule as precipitates grow would also explain the kinetic evolution of the system with PRC. A decrease in porosity implies a reduction of the specific surface area, which would achieve its minimal value at the granule surface. Therefore, as the porosity is clogged up, the kinetic rate drops.

In contrast, SEM examination of granules collected at the inlet (bottom) of Column 2 evidences entirely different processes (Figure 7(d) and 7(e)). A deposit about 140  $\mu\text{m}$  thick has coated the external surface of the granules. Furthermore, the clogging of the internal porosity that was previously observed for Column 1 is not present here (Figure S4). EDX line graphs of the deposit indicate that the average Ca/P molar ratio is  $1.64 \pm 0.14$ , which is consistent with a HAP precipitate. However, the obvious growth lines in the deposit associated with variations of Ca/P ratio in the 1.4–1.8 range, suggest that other forms of CaP phase might precipitate such as TCP, OCP and carbonated apatite. In particular, carbonation of apatite seems to occur and is represented by each dark growth line (Figure 7(e)). Slight changes in solution conditions may



**Figure 7** | SEM micrographs of polished cross-sections of the granules in Column 1 (mean PRC = 10 g P-PO<sub>4</sub> · kg<sup>-1</sup>). (a-b) Clogged regions close to the edge of granules examined in the secondary electron mode at (a) the bottom of the column, (b) the top of the column; (c-d) corresponding micrographs in the backscattered electron mode, the regions in light grey colour identifying the clogged porosity at (c) the bottom of the column, (d) the top of the column; SEM images of a pellet from the bottom of Column 2 showing a deposit of CaP, (e-f): detail of the surface of the granule at a mean PRC = 6.2 g P-PO<sub>4</sub> · kg<sup>-1</sup>, (e); detail of a polished cross-section enlarged at the edge of the pellet at a mean PRC = 10.9 g P-PO<sub>4</sub> · kg<sup>-1</sup>.

affect the continuity of the growing crystal, leading to changes in composition of the solid solution. Presumably the most recent precipitation layer (external) corresponds to Stage 2, where Ca concentration is reduced and thus the molar ratio C/Ca increases, leading to a more carbonated precipitate. Nevertheless, further experiments would be necessary to establish relationships between solution conditions and the evolution of the precipitates.

Unlike samples taken near the inlet of the system, no precipitation process could be observed in the samples collected from the media layers close to the outlet of the filter in Column 2 (Figure S5(b)), although the occurrence of adsorption cannot be dismissed. For the middle media layers, no SEM analyses were conducted; however, it would be likely that retention processes such as those seen for Column 1 occurred at some levels in the column with decreasing supersaturation. This results in a sharper PRC

gradient with HRT where the major P retention occurred in the first centimeters of the filter. Indeed, crystal growth requires a lower energy barrier to be exceeded than the formation of new nuclei. As supersaturation becomes lower with increasing HRT, the energy barrier to form new nuclei is higher. Therefore, the decline in the kinetic rate with PRC may be related to a reduction of the media porosity (or SSA) close to the inlet of the system.

## CONCLUSIONS

Two long-term column experiments for phosphorus retention with granulated apatite filters were conducted and assessed using the  $k-C^*$  model. The results showed unexpected low  $k_v$  values during precipitation (in the range of 0.63 h<sup>-1</sup> to 0.23 h<sup>-1</sup>) and low estimated values of maximum

PRC (10.5 and 12.4 g P-PO<sub>4</sub>·kg<sup>-1</sup> of material) compared with those of natural apatite. Such a result would prevent the granulated apatite filters ensuring an appropriate long-term performance. The k-C\* model presents some limitations and is not capable of representing processes' variations (depending on environmental conditions) and their associated kinetics. A mechanistic model would be necessary in such a case.

Mechanistic differences with respect to natural apatite were identified by the examination of SEM micrographs coupled with EDXS microanalyses. The binder matrix used for granulation hinders the access to the surface of apatite particles, which are then less likely to act as seeds for precipitation. As a consequence, calcium concentration, which affects the supersaturation of the inlet solution, appears to be the predominant parameter affecting the retention processes. For calcium concentrations around 70 mg·L<sup>-1</sup>, a lower supersaturation was attained, enabling diffusion of ions through the granule porosity which adsorb and precipitate at the binder matrix, all through the filter. The precipitation of hydroxyapatite may result in this case from two different processes: (1) seeded precipitation onto micrometric apatite particles; (2) precipitation promoted by local increases in supersaturation caused by the dissolution of calcium from the binder. In contrast, for calcium concentrations around 113 mg·L<sup>-1</sup>, the supersaturation of the solution close to the inlet of the system appeared to be high enough to promote heterogeneous nucleation onto the granules surface. The deposit showed different layers of precipitates as hydroxyapatite and carbonated hydroxyapatite. The samples close to the outlet of the system did not show the formation of any deposit, although adsorption into the matrix is suspected to occur.

Finally, it appeared that two major causes were responsible for the decrease in the kinetic rate of phosphorus retention: (1) the reduction of the SSA available with increasing PRC; (2) the decrease of supersaturation either through the column due to ion retention or inside the granules due to less Ca dissolution from the binder.

In conclusion, this work used laboratory column experiments conducted for more than a year to evaluate the capacity of this new material for phosphorus retention from wastewater. Despite granulated apatite has potentially the capacity for phosphorus retention, results showed worse performances and kinetics than natural apatites derived from its own configuration and the way they are manufactured. This will inevitably result in a high frequency of bed renewal, which may not be interesting from an economic point of view. The authors recommend addressing future

research efforts to enhance the comprehension of phosphorus retention processes on natural apatites and their hydraulic limitations for wastewater treatment applications.

## ACKNOWLEDGEMENTS

The authors want to thank Dr François Besueille and Ruben Vera from Institute of Analytical Science for their kind help. French Water Agencies Adour-Garonne and Rhône-Méditerranée-Corse provided financial support for this study.

## DATA AVAILABILITY STATEMENT

All relevant data are included in the paper or its Supplementary Information.

## REFERENCES

- Anderson, M. A. & Rubin, A. J. 1981 *Adsorption of Inorganics at Solid-Liquid Interfaces*. Ann Arbor Science, Ann Arbor, MI.
- Barone, J. P. & Nancollas, G. H. 1977 *The seeded growth of calcium phosphates. The effect of solid/solution ratio in controlling the nature of the growth phase*. *Journal of Colloid and Interface Science* **62** (3), 421–431. doi:10.1016/0021-9797(77)90093-5.
- Bellier, N., Chazarenc, F. & Comeau, Y. 2006 *Phosphorus removal from wastewater by mineral apatite*. *Water Research* **40** (15), 2965–2971. doi:10.1016/j.watres.2006.05.016.
- Blanco, I., Molle, P., Saenz de Miera, L. E. & Ansola, G. 2016 *Basic oxygen furnace steel slag aggregates for phosphorus treatment. Evaluation of its potential use as a substrate in constructed wetlands*. *Water Research* **89**, 355–365. doi:10.1016/j.watres.2015.11.064.
- Blandin, A. F. 2013 *Matériau granulaire à base de phosphate, son procédé de fabrication et son utilisation dans un dispositif de déphosphatation des eaux usées (Phosphate Based Granular Material, Process for Manufacturing Same and use Thereof in A Device for Removing Phosphates From Wastewater)*. O. M. d. I. P. Intellectuelle, Compagnie financière et de participations Roullier.
- Bouwman, A. F., Van Drecht, G., Knoop, J. M., Beusen, A. H. W. & Meinardi, C. R. 2005 *Exploring changes in river nitrogen export to the world's oceans*. *Global Biogeochemical Cycles* **19** (1). doi:10.1029/2004gb002314.
- Han, C., Wang, Z., Wu, Q., Yang, W., Yang, H. & Xue, X. 2016 *Evaluation of the role of inherent Ca(2+) in phosphorus removal from wastewater system*. *Water Science and Technology* **73** (7), 1644–1651. doi:10.2166/wst.2015.642.
- Harouiya, N., Martin Rue, S., Prost-Boucle, S., Liénar, A., Esser, D. & Molle, P. 2011 *Phosphorus removal by apatite in horizontal flow constructed wetlands for small communities:*

- pilot and full-scale evidence. *Water Science and Technology* **63** (8), 1629–1637. doi:10.2166/wst.2011.250.
- Kadlec, R. H. & Wallace, S. D. 2009 *Treatment Wetlands*. CRC Press, Boca Raton, FL.
- Martinez-Carvajal, G. D., Oxarango, L., Adrien, J., Molle, P. & Forquet, N. 2019 Assessment of X-ray computed tomography to characterize filtering media from vertical flow treatment wetlands at the pore scale. *Science of the Total Environment* **658**, 178–188. doi:10.1016/j.scitotenv.2018.12.119.
- Molle, P., Liénard, A., Grasmick, A., Iwema, A. & Kabbabi, A. 2005 Apatite as an interesting seed to remove phosphorus from wastewater in constructed wetlands. *Water Science & Technology* **51** (9), 193–203.
- Molle, P., Martin, S., Esser, D., Besnault, S., Morlay, C. & Harouiya, N. 2011 Phosphorus removal by the use of apatite in constructed wetlands: design recommendations. *Water Practice and Technology* **6** (3), wpt2011046. doi:10.2166/wpt.2011.046.
- Montastruc, L., Azzaro-Pantel, C., Biscans, B., Cabassud, M. & Domenech, S. 2003 A thermochemical approach for calcium phosphate precipitation modeling in a pellet reactor. *Chemical Engineering Journal* **94** (1), 41–50. doi:10.1016/s1385-8947(03)00044-5.
- Parkhurst, D. L. & Appelo, C. A. J. 2013 *Description of Input and Examples for PHREEQC Version 3—A Computer Program for Speciation, Batch-Reaction, One-Dimensional Transport, and Inverse Geochemical Calculations, U.S. Geological Survey*. U.S. Geological Survey Techniques and Methods: 497.
- Peng, L., Dai, H., Wu, Y., Peng, Y. & Lu, X. 2018 A comprehensive review of phosphorus recovery from wastewater by crystallization processes. *Chemosphere* **197**, 768–781. doi:10.1016/j.chemosphere.2018.01.098.
- Prieto, M., Heberling, F., Rodríguez-Galán, R. M. & Brandt, F. 2016 Crystallization behavior of solid solutions from aqueous solutions: an environmental perspective. *Progress in Crystal Growth and Characterization of Materials* **62** (3), 29–68. doi:10.1016/j.pcrysgrow.2016.05.001.
- Prochaska, C. A. & Zouboulis, A. I. 2006 Removal of phosphates by pilot vertical-flow constructed wetlands using a mixture of sand and dolomite as substrate. *Ecological Engineering* **26** (3), 293–303. doi:10.1016/j.ecoleng.2005.10.009.
- Song, Y., Hahn, H. H. & Hoffmann, E. 2002a The effect of carbonate on the precipitation of calcium phosphate. *Environmental Technology* **23** (2), 207–215. doi:10.1080/09593332508618427.
- Song, Y., Hahn, H. H. & Hoffmann, E. 2002b Effects of solution conditions on the precipitation of phosphate for recovery. *Chemosphere* **48** (10), 1029–1034. doi:10.1016/s0045-6535(02)00183-2.
- van Puijenbroek, P., Beusen, A. H. W. & Bouwman, A. F. 2019 Global nitrogen and phosphorus in urban waste water based on the shared socio-economic pathways. *Journal of Environmental Management* **231**, 446–456. doi:10.1016/j.jenvman.2018.10.048.
- Van Santen, R. A. 1984 The Ostwald step rule. *The Journal of Physical Chemistry* **88** (24), 5768–5769. doi:10.1021/j150668a002.
- Vohla, C., Kõiv, M., Bavor, H. J., Chazarenc, F. & Mander, Ü. 2011 Filter materials for phosphorus removal from wastewater in treatment wetlands – a review. *Ecological Engineering* **37** (1), 70–89. doi:10.1016/j.ecoleng.2009.08.003.
- Yang, Y., Zhao, Y., Liu, R. & Morgan, D. 2018 Global development of various emerged substrates utilized in constructed wetlands. *Bioresource Technology* **261**, 441–452. doi:10.1016/j.biortech.2018.03.085.

First received 26 August 2020; accepted in revised form 22 December 2020. Available online 7 January 2021